

The hadal zone is an important and heterogeneous sink of black carbon in the ocean

Xi Zhang^{1,14}, Yunping Xu^{1,2,14}✉, Wenjie Xiao^{1,3,14}✉, Meixun Zhao⁴, Zicheng Wang⁴, Xuchen Wang^{4,5}, Liping Xu⁵, Min Luo¹, Xinxin Li³, Jiasong Fang¹, Yin Fang¹, Yasong Wang¹, Kazumasa Oguri^{6,7}, Frank Wenzhöfer^{6,8,9}, Ashley A. Rowden^{10,11}, Siddhartha Mitra¹² & Ronnie N. Glud^{6,13}

Black carbon is ubiquitous in the marine environment. However, whether it accumulates in the deepest ocean region, the hadal zone, is unknown. Here we measure the concentration and carbon isotopes ($\delta^{13}\text{C}$ and $\Delta^{14}\text{C}$) of black carbon and total organic carbon in sediments from six hadal trenches. Black carbon constituted 10% of trench total organic carbon, and its $\delta^{13}\text{C}$ and $\Delta^{14}\text{C}$ were more negative than those of total organic carbon, suggesting that the black carbon was predominantly derived from terrestrial C3 plants and fossil fuels. The contribution of fossil carbon to the black carbon pool was spatially heterogeneous, which could be related to differences in the distance to landmass, land cover and socioeconomic development. Globally, we estimate a black carbon burial rate of $1.0 \pm 0.5 \text{ Tg yr}^{-1}$ in the hadal zone, which is seven-fold higher than the global ocean average per unit area. We propose that the hadal zone is an important, but overlooked, sink of black carbon in the ocean.

¹ Shanghai Frontiers Research Center of the Hadal Biosphere & HAST, College of Marine Sciences, Shanghai Ocean University, Shanghai 201306, China.

² State Key Laboratory of Estuarine and Coastal Research, East China Normal University, Shanghai 200241, China. ³ Department of Ocean Science and Engineering, Southern University of Science and Technology, Shenzhen 518055, China. ⁴ Frontiers Science Center for Deep Ocean Multispheres and Earth System, and Key Laboratory of Marine Chemistry Theory and Technology, Ministry of Education, Ocean University of China, Qingdao 266100, China.

⁵ Center for Isotope Geochemistry and Geochronology, Qingdao National Laboratory for Marine Science and Technology, Qingdao 266237, China.

⁶ Department of Biology, Hadal, Nordcee & DIAS, University of Southern Denmark, 5230 Odense M, Denmark. ⁷ Research Institute for Global Change, Japan Agency for Marine-Earth Science and Technology, 2-15 Natsushima, Yokosuka, Kanagawa 237-0061, Japan. ⁸ HGF-MPG Group for Deep Sea Ecology & Technology, Alfred Wegener Institute Helmholtz Centre for Polar- and Marine Research, Am Handelshafen 12, 27570 Bremerhaven, Germany. ⁹ Max Planck Institute for Marine Microbiology, Celsiusstr 1, D-28359 Bremen, Germany. ¹⁰ Coast and Oceans National Centre, National Institute of Water & Atmosphere Research (NIWA) Ltd, Private Bag 14901, Kilbirnie 6241, Wellington, New Zealand. ¹¹ School of Biological Sciences, Victoria University of Wellington, PO Box 600, Wellington 6140, New Zealand. ¹² Geological Sciences, East Carolina University, Greenville, NC 27858, USA. ¹³ Department of Ocean and Environmental Sciences, Tokyo University of Marine Science and Technology, 26 108-8477, Tokyo, Japan. ¹⁴ These authors contributed equally: Xi Zhang, Yunping Xu, Wenjie Xiao. ✉email: ypxu@shou.edu.cn; wjxiaocug@126.com

Black carbon (BC) is highly condensed carbonaceous residue mainly from incomplete combustion processes^{1,2}. The modern annual emissions from combustion of fossil fuel and burning of terrestrial biomass are 6.6–7.2 Tg (10¹² g)³ and 196–340 Tg, respectively⁴. Due to its refractory aromatic structures, BC has a long environmental lifetime⁵, providing sufficient time for BC to reach remote oceans^{6,7}. The BC burial flux in ocean sediments was estimated to be 10.3 Tg yr⁻¹, of which only 0.6 Tg yr⁻¹ was accumulated in deep-sea sediments⁸. However, the BC to total organic carbon (TOC) ratio (BC/TOC) in deep-sea sediments is usually higher than that in continental shelf sediments⁹. Once deposited in deep sea, BC escapes from photodegradation and is relatively resistant to microbial degradation, thus representing an important slow-cycling carbon retention¹⁰. Previous studies have reported the BC in sublittoral, bathyal and abyssal zones (water depth <6000 m)^{6,8,10–12}, but no data exist for sediments in the hadal zone (water depth of 6000–11,000 m). A recent study¹³ examined dissolved BC in waters from Mariana Trench (MT) and found that it is cycled and aged on the same time scales as bulk dissolved organic carbon (OC) in the ocean. This finding, however, is not consistent with the prevailing view that the BC was thought to be a refractory pool of carbon with much old ¹⁴C ages (~20,000 yr BP)^{10,14}.

The hadal zone is mainly composed of trenches formed at the subduction zones. Despite representing only ~1% of total seafloor area, the hadal zone accounts for 45% of the ocean's depth range^{15,16}. Hadal trench ecosystems are one of the least explored habitats on Earth due to extreme challenges of sampling¹⁵. Recent studies have suggested that elevated OC accumulation rates^{17,18}, benthic abundance and biomass^{19,20}, and microbial activities^{21–23} are prevalent in some hadal trenches. These characteristics have been attributed to the funneling effect of hadal trenches due to unique V-shaped topography, further facilitated by occasional seismic activities and high-frequency fluid dynamics^{18,24,25}. As an example, >7 Tg of OC has been remobilized from surficial slope sediments and exported to the hadal realm of the Japan Trench by earthquakes in the past 2000 years²⁶, confirming the importance of hadal trenches as accumulation regions for OC in the deep sea. Given a close relationship between BC and TOC contents in marine sediments⁷, we hypothesize that large amount of BC has been accumulated in the hadal zone.

Here, we collected sediment samples from the six hadal trench regions (hadal sites and surrounding non-hadal sites), including MT, Mussau Trench (MST), New Britain Trench (NBT), Bougainville Trench (BT), Kermadec Trench (KT) and Atacama Trench (AT) (Fig. 1; Supplementary Table 1). BC was quantified using the chemothermal oxidation-375 (CTO-375) method. We also measured stable and radioactive carbon isotopes ($\delta^{13}\text{C}$ and $\Delta^{14}\text{C}$) of BC and TOC using isotope ratio mass spectrometry and accelerator mass spectrometry (AMS), respectively. The $\delta^{13}\text{C}$ enables distinguishing OC from terrestrial C3 plants, C4 plants and marine phytoplankton, which have an average $\delta^{13}\text{C}$ signature of $-27.1 \pm 2.0\%$, $-13.1 \pm 1.2\%$ and $-20 \pm 1.0\%$, respectively^{27,28}. Since there is only minor isotopic fractionation between the product of vegetation burning and original vegetation biomass (1–2‰)²⁹, the $\delta^{13}\text{C}$ signature of BC is a reliable source indicator. In addition, the $\Delta^{14}\text{C}$ is indicative of the contributions of biomass burning versus fossil carbon combustion to the BC pool because fresh biomass has a modern radiocarbon age ($\Delta^{14}\text{C} \geq 0$), whereas fossil carbon is completely devoid of radiocarbon ($\Delta^{14}\text{C} = -1000\%$)^{30,31}. Based on the contents, $\delta^{13}\text{C}$ and $\Delta^{14}\text{C}$ signatures of both BC and TOC, and ²¹⁰Pb-derived sedimentation rates, we hereby attempt to determine the concentration, source, and distribution of BC in the hadal trenches, and to assess the role of the hadal zone for BC burial in the global ocean.

Results

Content, $\delta^{13}\text{C}$ and $\Delta^{14}\text{C}$ of TOC in trench surface sediments. The content, $\delta^{13}\text{C}$ and $\Delta^{14}\text{C}$ of BC and TOC in trench surface sediments are summarized in Supplementary Table 2. The TOC content (expressed as weight percentage of TOC to sediment; same hereafter) ranged from 0.15% to 2.39%, with an average of 0.31% in MT, 0.57% in MST, $0.45 \pm 0.18\%$ in NBT, $0.26 \pm 0.08\%$ in BT, $0.24 \pm 0.09\%$ in KT, and $0.87 \pm 0.58\%$ in AT. The $\delta^{13}\text{C}$ values of sedimentary TOC varied between -24.4% and -19.9% , with an average of -20.0% in MT, -20.0% in MST, $-22.0 \pm 1.6\%$ in NBT, $-20.7 \pm 1.0\%$ in BT, $-23.1 \pm 0.4\%$ in KT, and $-22.0 \pm 1.0\%$ in AT. The $\Delta^{14}\text{C}$ values of sedimentary TOC ranged from -891% to -82% , corresponding to ¹⁴C ages of 17,790 to 690 yr BP. For each trench, the $\Delta^{14}\text{C}$ of sedimentary TOC was -391% in MT, -418% in MST, $-172 \pm 65\%$ in NBT, $-224 \pm 126\%$ in BT, $-683 \pm 157\%$ in KT, and $-446 \pm 151\%$ in AT.

Content, $\delta^{13}\text{C}$ and $\Delta^{14}\text{C}$ of BC in trench surface sediments. The BC content ranged from 0.011% to 0.18%, with an average of 0.013% in MT, 0.071% in MST, $0.024 \pm 0.009\%$ in NBT, $0.014 \pm 0.002\%$ in BT, $0.036 \pm 0.007\%$ in KT, and $0.077 \pm 0.046\%$ in AT. The $\delta^{13}\text{C}$ of BC varied between -27.7% and -22.3% , with an average of -24.3% in MT, -24.0% in MST, $-23.7 \pm 0.9\%$ in NBT, $-25.9 \pm 0.9\%$ in KT, and $-25.7 \pm 1.0\%$ in AT. Note the lack of BC- $\delta^{13}\text{C}$ data for BT due to insufficient samples. The $\Delta^{14}\text{C}$ of BC ranged from -893% to -346% , corresponding to ¹⁴C ages of 17,870 to 3340 yr BP. For each trench, the $\Delta^{14}\text{C}$ of sedimentary TOC was -626% in MT, -661% in MST, $-473 \pm 77\%$ in NBT, $-415 \pm 49\%$ in BT, $-729 \pm 105\%$ in KT and $-694 \pm 164\%$ in AT.

Depth profiles of TOC and BC in trench core sediments. More extensive investigations were conducted for two cores from the landward abyssal site (A9) and hadal axis site (A10). The TOC, BC, $\delta^{13}\text{C}$ and $\Delta^{14}\text{C}$ of these cores were measured down to a depth of 15 and 35 cm, respectively, and the results are summarized in Supplementary Tables 3 & 4. In the core from site A9, the TOC and BC contents varied from 0.90% to 1.56% and 0.11% to 0.20%, respectively, whereas the $\delta^{13}\text{C}$ fell in a narrow range for TOC (-21.7% to -21.1%) and BC (-26.6% to -25.9%). The sediments from surface (0–1 cm), middle (5–6 cm) and deep (9–10 cm) layers, respectively, had $\Delta^{14}\text{C}$ values of -319% , -434% and -760% for TOC, and -457% , -453% and -767% for BC. In the core from site A10, the TOC and BC content ranged from 1.01% to 2.07%, and 0.09% to 0.18%, respectively. Like the core from site A9, one from site A10 has a relatively narrow range of $\delta^{13}\text{C}$ values for TOC (-22.2% to -21.2%) and BC (-26.4% to -25.6%). The sediments at 0–1 cm, 7–8 cm, 17.5–20 cm and 30–35 cm layers, respectively, had $\Delta^{14}\text{C}$ values of -311% , -332% , -341% and -403% for TOC, and -430% , -386% , -411% and -502% for BC.

Discussion

A weak but still significant correlation was observed between the BC and TOC contents ($r = 0.43$, $p < 0.05$; Fig. 2a). The inter-trench comparison revealed that the BC content was the highest in AT ($0.077 \pm 0.046\%$) compared to KT ($0.036 \pm 0.007\%$), NBT ($0.024 \pm 0.009\%$) and BT ($0.014 \pm 0.002\%$) (Fig. 3a). Correspondingly, the AT had the highest TOC content ($0.87 \pm 0.58\%$), followed by NBT ($0.45 \pm 0.18\%$), BT ($0.26 \pm 0.01\%$) and KT ($0.24 \pm 0.09\%$) (Fig. 3b). The fact that we only have one sample from MST and MT prevented a robust inter-trench comparison including these two trenches, and thus they have been omitted for this part of the discussion. The highest BC/TOC ratio occurred in KT (0.17 ± 0.05),

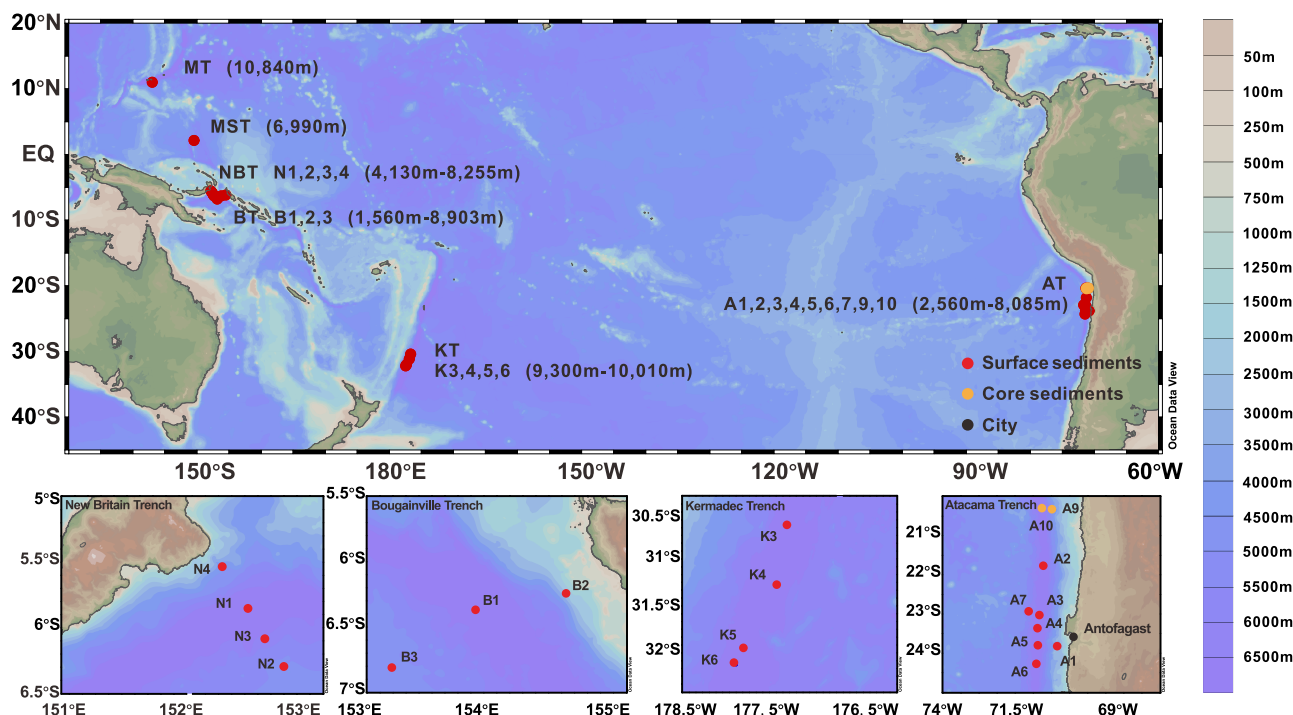


Fig. 1 Map showing sampling sites of six trench regions in the Pacific Ocean. The site information is summarized in Supplementary Table 1. The numbers in bracket denote water depth range at each trench. MT Mariana Trench, MST Mussau Trench, NBT New Britain Trench, BT Bougainville Trench, KT Kermadec Trench, AT Atacama Trench. Base map was drawn using the Ocean Data View software package⁶³.

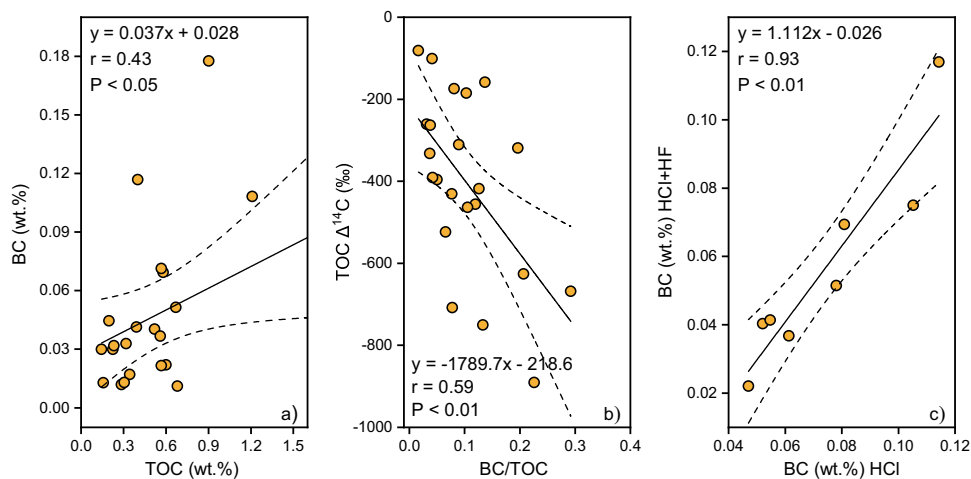


Fig. 2 Linear correlations for different types of carbon in surface sediments from six trench regions. **a** Total organic carbon (TOC) and black carbon (BC) contents. **b** TOC radioactive carbon isotopic composition ($\Delta^{14}C$) and BC/TOC ratio. **c** BC contents with and without hydrofluoric acid (HF)-treatments. The dotted lines are 95% credible intervals.

followed by AT (0.11 ± 0.08), NBT (0.074 ± 0.049) and BT (0.058 ± 0.017) (Fig. 3c). The KT underlies mesotrophic surface waters (Net primary productivity: $135\text{--}152 \text{ g C m}^{-2} \text{ yr}^{-1}$) that are expected to export moderate amount of marine OC to the seafloor³². The closest countries to the KT are industrialized countries that use fossil fuel primarily for transport (New Zealand) and for the production of electricity (Australia). Thus, the KT may receive substantial amounts of BC from fossil fuel combustion, a notion that is supported by relatively old radiocarbon age of the BC in KT (Fig. 4a). In AT, strong upwelling has induced high net primary productivity ($306\text{--}449 \text{ g C m}^{-2} \text{ yr}^{-1}$) that is suspected to export large amount of marine OC (non-BC) to the seafloor, while Atacama Desert, one of the most arid region of the world, supplied little fresh terrestrial OC³³. In addition, most AT sites are close to

Antofagasta, a harbor city in northern Chile (Fig. 1). This city, plus mining activities in Atacama Desert³⁴, could produce BC from fossil fuel combustion and rock weathering that was transported to AT by prevailing westerly wind. Taken together, high marine primary productivity, the lack of vegetation cover and important emission of fossil BC result in an intermediate BC/TOC content in AT sediments. The lowest BC/TOC ratio occurring in the BT and NBT regions suggests that sedimentary TOC is mainly derived from non-BC OC such as phototrophic marine products from phytoplankton and terrestrial materials from tropical forests in adjacent Papua New Guinea³⁵. This finding is consistent with less BC emission from fossil fuel combustion in less industrialized Papua New Guinea as compared to more industrialized countries like New Zealand and Australia¹³.

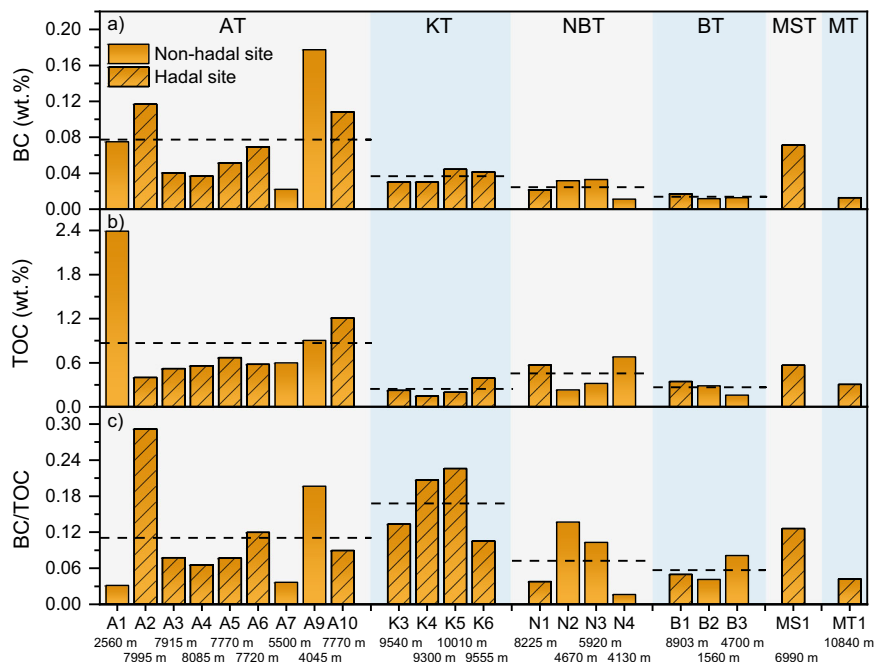


Fig. 3 Summary results of black carbon (BC) content, total organic carbon (TOC) content, and BC/TOC ratio in surface sediments from six trench regions. a BC content. **b** TOC content. **c** BC/TOC ratio. AT Atacama Trench, BT Bougainville Trench, KT Kermadec Trench, MST Mussau Trench, MT Mariana Trench, NBT New Britain Trench. The dash lines denote average values of the parameters in each trench.

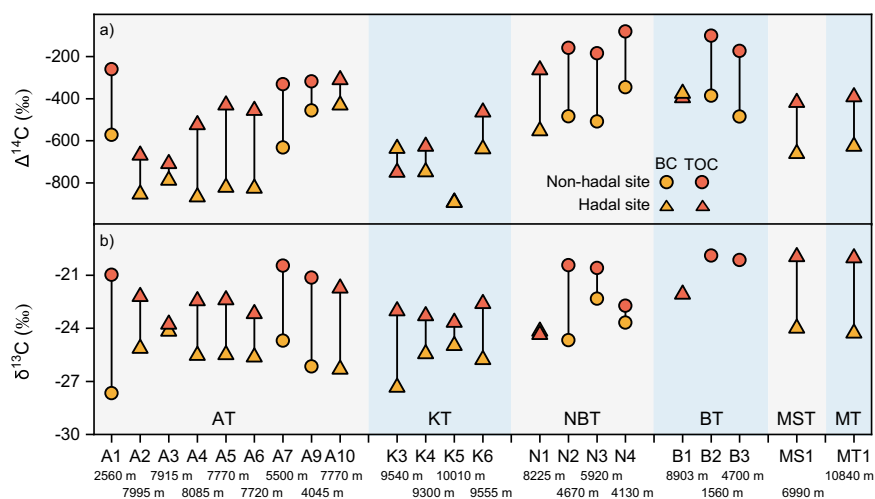


Fig. 4 Offset of carbon isotopic compositions between black carbon (BC) and total organic carbon (TOC) in surface sediments from six trench regions. a radioactive carbon isotopic composition ($\Delta^{14}\text{C}$). **b** stable carbon isotopic composition ($\delta^{13}\text{C}$). AT Atacama Trench, BT Bougainville Trench, KT Kermadec Trench, MST Mussau Trench, MT Mariana Trench, NBT New Britain Trench. Note the $\delta^{13}\text{C}$ data of the BC at sites B1, B2 and B3 (BT) are not available.

Along each trench axis, the BC content and BC/TOC ratio, respectively, varied in a range of 0.04–0.12% ($0.07 \pm 0.03\%$) and 0.078–0.29 (0.12 ± 0.08) in AT (A2–A6, A10), and 0.03–0.05% ($0.04 \pm 0.01\%$) and 0.13–0.23 (0.17 ± 0.05) in KT (K3–K6) (Fig. 3c). Previous studies have reported high heterogeneity of sedimentary TOC in Yap Trench³⁶, NBT^{37,38}, MT²¹, KT and AT³⁹. However, to the best of our knowledge, our study is the first report for the heterogenous distribution of BC in hadal trenches. This feature is likely attributed to complex environmental processes due to turbidity currents⁴⁰, internal tides²⁴ and complex bathymetry within trench interiors⁴¹. The site-to-site comparisons of the BC content between hadal and non-hadal surface sediments (i.e., A1 vs. A5; A3 vs. A7; A9 vs. A10) tend to decrease from landward bathyal/abyssal sites (A1, A9) to hadal axis sites (A3, A5, A10) and then to oceanward abyssal site (A7) (Fig. 3a).

This seaward decrease suggests that the BC preserved in the AT region is primarily from its adjacent land on the east (i.e., Chile). In contrast, in the NBT and BT regions, the BC content does not show a decreasing trend from landward site to hadal axis site and then to oceanward site (i.e., N4–N1–N3–N2, and B2–B1–B3; Fig. 3a), suggesting that the BC input is not only from New Britain Island and Bougainville Island on the north, but also likely from the mainland of Papua New Guinea on the south.

The $\delta^{13}\text{C}$ of BC in surface sediments in AT (-27.7% to -24.2%) and KT (-27.3% to -25.0%) is more negative than that in NBT (-24.7% to -22.3%) ($p < 0.01$), MT (-24.3%) and MST (-24.0%) (Fig. 4b), presumably reflecting inter-trench variability in the BC sources (e.g., biomass burning from different type plants or combustion of different fossil fuels)^{13,28,42}. While within each trench (i.e., AT), BC $\delta^{13}\text{C}$ values do not show

significant difference between hadal and non-hadal sediments (-26.3‰ to -24.2‰ vs. -27.7‰ to -24.7‰) ($p > 0.05$). Taking all surface sediments together, the average BC $\delta^{13}\text{C}$ value ($-25.1 \pm 1.2\text{‰}$) is significantly more negative than average TOC $\delta^{13}\text{C}$ value ($-21.9 \pm 1.4\text{‰}$; Fig. 4b) ($p < 0.01$), suggesting different sources between BC (predominant terrestrial source) and co-deposited TOC (predominant marine source). Such $\delta^{13}\text{C}$ offset between BC and TOC was also found in marine sediments from South Atlantic (-23‰ to -27‰ vs. -18‰ to -24‰)⁶ and the Santa Monica Basin (-24.2‰ to -25.0‰ vs. -21.5‰ to -23.5‰)⁴³.

Interestingly, oceanic dissolved BC, unlike sedimentary BC, presents less negative $\delta^{13}\text{C}$ signature similar to that of marine phytoplankton. For example, the $\delta^{13}\text{C}$ of BC in MT sediment is -24.3‰ (this study), whereas that of dissolved BC in MT waters (8000–10,000 m) varies between -20.4‰ and -18.9‰ ¹³. At the ocean basin scale, the $\delta^{13}\text{C}$ of sedimentary BC in six trench regions is $-25.1 \pm 1.2\text{‰}$, while that of dissolved BC in Pacific and Atlantic oceans ranges from -22.9‰ to -24.3‰ ⁴⁴. This difference may reflect different sources and/or biogeochemical processes between dissolved and sedimentary BC. The result based on the benzene polycarboxylic acid method revealed that oceanic dissolved BC was 6–8‰ enriched in ^{13}C compared to riverine dissolved BC⁴⁴, while that based on the CTO-375 method also showed that dissolved BC became enriched in ^{13}C from rivers (-26.4‰ to -22.6‰) to ocean (-20.9‰ to -18.4‰)¹³. This positive shift in $\delta^{13}\text{C}$ suggests that oceanic dissolved BC either is predominantly derived from a non-riverine source or undergoes isotopic fractionation potentially associated with photo- and biodegradation. Currently, there is no direct evidence supporting conservative or nonconservative behaviors of BC $\delta^{13}\text{C}$ during transport and mixing into the ocean, but a large fraction of riverine dissolved BC could be degraded before it reaches open ocean¹³. Note that the methods like the benzene polycarboxylic acid and CTO-375 have different analytical windows for BC (non-aromatic, condensed aromatic and graphitic fractions)⁴⁵, and their results are not completely overlapping. However, both Qi et al.¹³ and our study used the CTO-375 method for the BC in MT and the results still reveal distinct $\delta^{13}\text{C}$ values between dissolved and sedimentary BC, suggesting that it is not the analytical methods that cause the $\delta^{13}\text{C}$ offset between oceanic dissolved and sedimentary BC. Considering an important mineral matrix on the fate of particulate organic matter in the ocean⁴⁶ and soil⁴⁷, we propose that the mineral protection may minimize the isotopic fractionation for particulate BC along the river to ocean continuum, whereas such protection mechanism is absent for dissolved BC. This hypothesis, however, needs to be tested in further work.

In 20 out of the 22 surface sediments, the BC $\Delta^{14}\text{C}$ values (-893‰ to -346‰) were more negative than the TOC $\Delta^{14}\text{C}$ values (-891‰ to -82‰) (Fig. 4a), corresponding to an average age offset of 3720 years. A negative correlation between the BC/TOC ratio and $\Delta^{14}\text{C}$ age of the TOC ($r = -0.59$; $p < 0.01$; Fig. 2b) suggests an important influence of the BC content on the bulk radiocarbon ages of sedimentary TOC and a negligible influence of charring during our pretreatment processes for BC analysis. The older age of BC relative to the co-deposited TOC was also found in Arctic sediments^{11,48}, Northeastern Pacific and Southern Ocean sediments¹⁰. Thus, the BC preserved in deep-sea sediments generally appeared to be of an older refractory carbon source compared to non-BC OC.

The distribution of the $\delta^{13}\text{C}$ versus $\Delta^{14}\text{C}$ of BC from the trench regions (this study) and other marine settings (previous studies) is depicted in Fig. 5. Overall, our BC data from hadal trenches are characterized by more depleted $\delta^{13}\text{C}$ compared to those from Arctic Ocean¹¹ and Washington coast (North Pacific Ocean)⁴²,

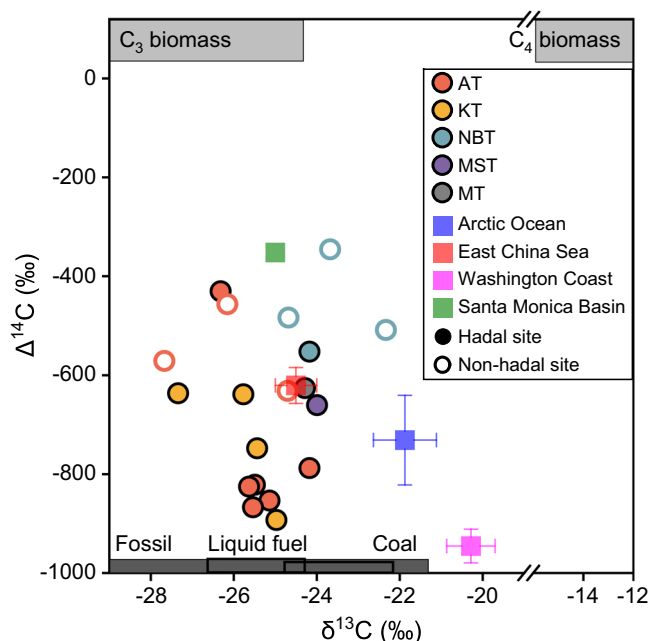


Fig. 5 Cross-plot of stable carbon isotopic composition ($\delta^{13}\text{C}$) and radioactive carbon isotopic composition ($\Delta^{14}\text{C}$) for the Black carbon (BC) in sediments. The data are from trench regions (this study) and Arctic Ocean¹¹, East China Sea¹², Washington coast (North Pacific Ocean)⁴², and Santa Monica Basin (North Pacific Ocean)⁴³. Error bars denote standard deviation.

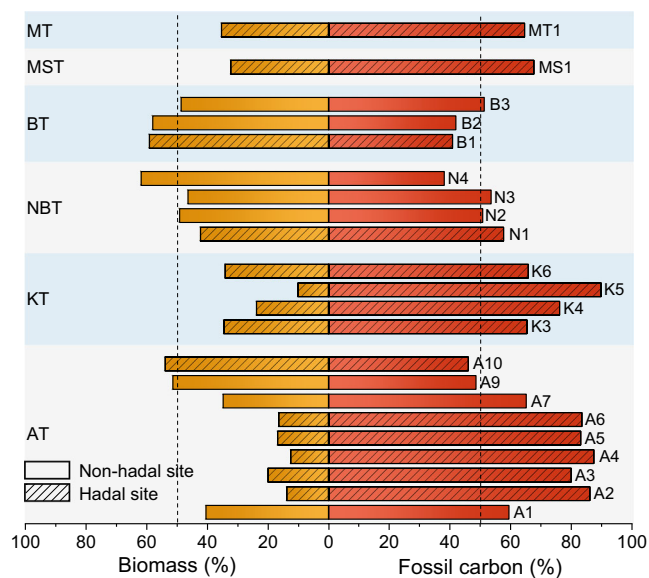


Fig. 6 Radioactive carbon isotopic composition ($\Delta^{14}\text{C}$)-based estimate for proportion (%) of fossil carbon and biomass burning to the Black carbon (BC) pool in surface sediments from six trench regions. AT Atacama Trench, BT Bougainville Trench, KT Kermadec Trench, MST Mussau Trench, MT Mariana Trench, NBT New Britain Trench. The vertical dash lines denote 50% contribution.

and more negative $\Delta^{14}\text{C}$ compared to those from the East China Sea¹² and Santa Monica Basin (North Pacific Ocean)⁴³. The application of $\Delta^{14}\text{C}$ -based two endmember mixing model shows apparent inter-trench variability in the BC source (Fig. 6). The proportion of fossil carbon (f_{fossil}) and biomass burning (f_{biomass})

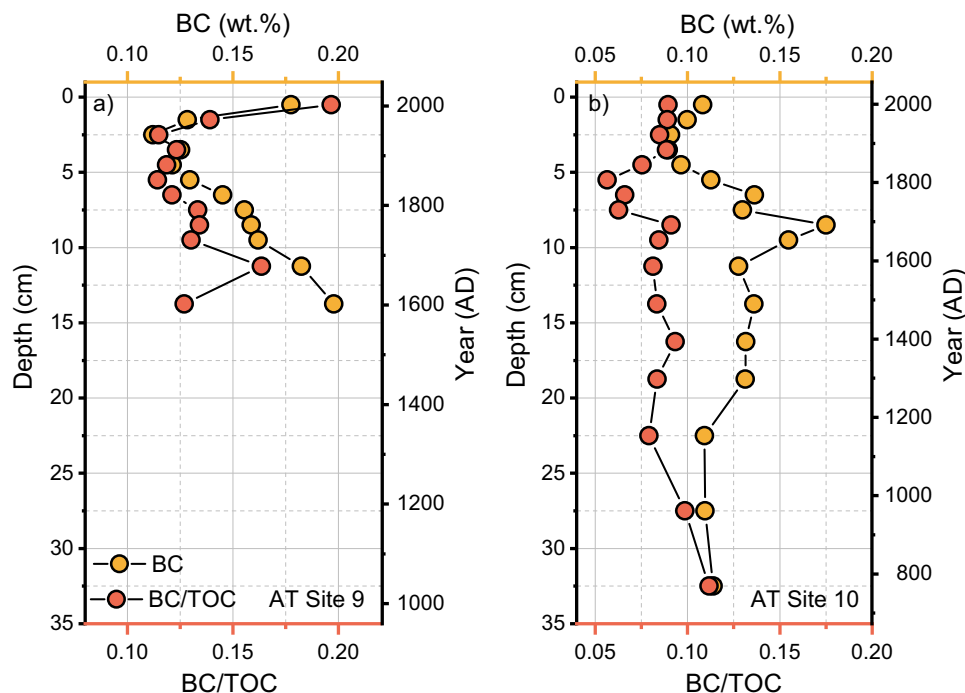


Fig. 7 Depth (Age) profiles of the Black carbon (BC) content and BC over total organic carbon (TOC) ratio in two sediment cores in the Atacama Trench (AT). **a** non-hadal site A9. **b** adjacent hadal site A10.

ranges from 38% to 90% ($64 \pm 16\%$) for f_{fossil} and 10% to 62% ($36 \pm 16\%$) for f_{biomass} . The mean f_{biomass} is the highest in the NBT and BT regions (50%, 56%), intermediate in the MST and MT regions (32%, 36%), and the lowest in the KT and AT regions (26%, 29%). This distribution pattern is consistent with the global ^{14}C dataset for atmospheric BC that shows larger biomass contributions in rural and less developed regions⁴⁹, such as the less industrialized Papua New Guinea close to NBT and BT, and larger fossil carbon contributions in more industrialized regions such as New Zealand and Australia as the nearest lands to KT. The low f_{biomass} in AT can be explained by the unique feature of its BC-source region (Atacama Desert) where the sparse vegetation contributed to little biomass burning derived BC, but the anthropogenic activities (e.g., mining and related industries) could produce the BC from rock weathering and fossil fuel combustion⁵⁰.

Both the hadal axis core site (A10) and landward abyssal core site (A9) display similar and stable $\delta^{13}\text{C}$ signals of the BC ($-26.1 \pm 0.3\text{‰}$ and $-26.2 \pm 0.3\text{‰}$, respectively), suggesting that BC is predominantly derived from C3 terrestrial plant material. The BC content and BC/TOC ratio, however, show some differences between the two cores. The core from site A9 is characterized by higher levels for both BC content ($0.15 \pm 0.03\%$) and BC/TOC ratio (0.14 ± 0.02) compared to that from site A10 ($0.12 \pm 0.02\%$ and 0.084 ± 0.013) ($p < 0.01$) (Fig. 7a). Such differences are likely caused by different distance to the BC source regions with the core from site 9 being closer to the shoreline of Chile. In this core, the BC content exhibits a decrease first and then an increase post-1940s (3–0 cm), whereas the BC/TOC ratio remains at a stable level until 1880 and increased afterwards that is coeval with increasing human activities in the 20th century. This profile, however, is not observed in the core from site A10 that does not show a clear trend except for a peak at ca. 1700 AD (9 cm) for the BC content and a drop during ca. 1730–1810 AD (8–6 cm) for the BC/TOC ratio (Fig. 7b)¹⁶. These abrupt changes may be caused by mass-wasting events, such as submarine landslides, because of the high seismicity^{17,50}. Nevertheless, the

BC content in surface sediments (0.18% in A9 and 0.11% in A10) is similar to an average level of respective core (0.15% in A9 and 0.12% in A10), suggesting that the BC content in surface sediments may represent a long-term average at this site. Using this rationale, we below estimate BC accumulation rates based on BC values of the surface sediments.

The BC preserved in marine sediments represents a long-term carbon sink for atmospheric CO_2 . The sedimentation rate obtained from regression of $^{210}\text{Pb}_{\text{ex}}$ (excess ^{210}Pb activity) versus core depth ranges from 0.026 to 0.20 cm yr^{-1} (Supplementary Table 5)¹⁶. Based on the data of sedimentation rate, BC content and dry sediment bulk density, we calculated the accumulation rate of BC in five trench regions, i.e., MT, NBT, BT, KT, and AT. The detailed calculation procedures are explicated in Supplementary Note 4. The results range from 0.07 to 0.48 $\text{g m}^{-2} \text{yr}^{-1}$ with an average value of $0.29 \pm 0.15 \text{ g m}^{-2} \text{yr}^{-1}$ for the BC accumulation rate (Table 1; Supplementary Table 6), which is comparable with that for the China continental shelf sea^{51,52}, but 2 order of magnitude greater than that for the open ocean sediments of the Pacific Ocean⁵³ and South Atlantic Ocean⁶ (Supplementary Table 7). Our finding of higher BC accumulation rates in the deepest trenches is consistent with previous studies that showed higher OC accumulation rates³⁸ and higher concentrations of pollutants⁵⁴ in the hadal zone relative to surrounding abyssal/bathyal zones. This characteristic is attributed to the hadal zone's V-shaped topography with steep slopes that can create gravity-driven downward transport, and even mass-wasting events occurred frequently in the hadal zone^{25,38,25}.

The quantification of the global BC burial in the hadal zone is still confounded by limited sampling and the heterogeneity of BC content among and within trenches. Nevertheless, our target trenches span a variety of geographically settings, i.e., MT and MST (low primary productivity and remote from lands), NBT/BT (moderate primary productivity and close to less developed country), KT (moderate primary productivity and remote from lands), and AT (high primary productivity and close to the developing country). We extrapolated the estimate from five

Table 1 Black carbon (BC) and total organic carbon (TOC) burial estimates in the hadal zone.

Trench	Area km ²	BC wt. %	TOC	SR cm yr ⁻¹	BC AR g m ⁻² yr ⁻¹	TOC AR	BC mean AR	TOC mean AR	BC flux in global hadal Tg yr ⁻¹	TOC flux in global hadal
AT	61000	0.070 ± 0.032	0.657 ± 0.260	0.046 ± 0.019	0.39 ± 0.09	393 ± 134	0.29 ± 0.15	5.2 ± 4.2	1.0 ± 0.5	17.7 ± 14.1
KT	120000	0.036 ± 0.007	0.240 ± 0.093	0.036 ± 0.006	0.19 ± 0.06	146 ± 0.85				
NBT	17000	0.022	0.568	0.160	0.48	12.73				
BT	12000	0.017	0.344	0.130	0.31	6.25				
MST	7800	0.071	0.567	-	-	-			10.2 ⁸	169 ⁶⁴
MT	110000	0.013	0.307	0.038	0.07	1.63			11.2	187
Global ocean	previous updated								8.7 ± 4.5%	9.5 ± 7.6%
Hadal zone (%)										

Sedimentation rate is obtained by regression of ²¹⁰Pb_{ex} (excess ²¹⁰Pb activity) versus core depth (Supplementary Table 5). Note sedimentation rate (SR) in the MST is not available (-). The BC and TOC flux in global hadal is calculated by multiplying respective accumulation rate (AR) of five trenches and total surface area of the hadal zone (3.4 × 10⁶ km²)¹⁶.
 AT Atacama Trench, BT Bougainville Trench, KT Kermadec Trench, MST Mussau Trench, MT Mariana Trench, NBT New Britain Trench.

trenches to the global hadal zone. MST is not included due to the unavailability of sedimentation rate data. Multiplying the number of five trenches by global hadal zone surface area (ca. 3.4 × 10⁶ km²)¹⁶ resulted in the accumulation rate of 1.0 ± 0.5 Tg yr⁻¹ (Table 1). This number is greater than previous estimate for the deep sea (0.6 Tg yr⁻¹) by about 70%⁸. Our result has updated the global marine BC accumulation rate from 10.2 Tg yr⁻¹ to 11.2 Tg yr⁻¹, of which the hadal zone is responsible for 8.7 ± 4.5%. Per unit area, the hadal zone, being ~1% of total seafloor area, has a BC burial rate greater than global ocean average by sevenfold. Note that our estimate does not consider episodic events such as earthquakes that could trigger mass-wasting events and transport enormous amounts of sediment and associated carbon into the hadal zone in a short time^{17,55}, suggesting that our estimate is conservative and likely lower than the actual BC burial flux in the hadal zone. Nevertheless, our estimate for the burial rate of TOC in the hadal zone (17.7 ± 14.1 Tg yr⁻¹; Table 1) is consistent with the previous estimate for the TOC subducted into the trenches based on global sediment cores from non-hadal sites adjacent to the subduction trenches (12 Tg yr⁻¹)⁵⁶. This consistency supports that our hadal sites-based estimate for TOC and BC burial rates is reasonable. Thus, the hadal zone is an important, but previously unrecognized sink for the BC in the deep ocean.

Methods

Sample collections. A series of short sediment cores (up to 40 cm) were collected from hadal and non-hadal sites of MT, MST, NBT, BT, KT and AT during three cruises (2016–2018) (Fig. 1). A part of cores was sliced, with representative sub-samples used in this study. The investigated trenches are in different biogeochemical provinces of the Pacific Ocean, characterized by different levels of net primary productivity (48–449 g C m⁻² yr⁻¹)³², water depth (1560–10,840 m) and terrestrial influences. The detailed sampling and site information is summarized in Supplementary Note 1 and Supplementary Table 1.

Pretreatment for TOC and BC measurements. Sediments were freeze-dried and homogenized in an agate mortar and pestle. 2–3 g of dry sediments was weighted into a 50-ml centrifuge tube and was mixed with excess 1 M hydrochloric acid (HCl) to remove inorganic carbon. After reaction for 24 h during which the samples were stirred for several times by a vortex stirrer, the sediments were centrifuged (3800 rpm, 10 min) and the supernatants were carefully removed by pipettes. The residue was further mixed with 20 ml ultrapure water (18.2 MΩ.cm). After centrifuged (3800 rpm, 10 min), the supernatant was again carefully removed. Repeat this step for three times until the pH was close to 7. The decarbonated sediments were freeze-dried and homogenized. Aliquots of decarbonated sediments (ca. 1 g) were used for analyses of content, δ¹³C and Δ¹⁴C of TOC and BC. However, some samples from the BT, KT and MT had extremely low BC contents, and were unable to be directly quantified for BC content. Thus, the decarbonated surface sediments (ca. 1 g) were further concentrated by reaction with excess hydrofluoric acid (HF) for 24 h. In order to avoid the loss of OC and BC, the HF-treated sediments were not rinsed with ultrapure water, and instead were dried at 60 °C prior to analyses of BC content.

Currently, there is no universally accepted method for quantifying BC content. The chemothermal oxidation method at 375 °C (CTO-375) is suitable for soot/graphitic BC in sediments and soils^{57,58}, which was used in our study. About 1 g (dry weight) of acid treated sediment was placed in a thin even layer (1–2 mm) in a crucible and heated at 375 °C for 24 h in an oven with continuous air supply. The residual carbon was operationally defined as BC⁵⁷. In order to test if the BC content was altered during HF treatment, we chose eight surface sediment samples that have relatively high BC contents, and compared their BC contents with and without HF-treatment (w/o HF). The results show a strong positive correlation: BC content with HCl + HF (%) = 1.112 × BC content with HCl (%) – 0.026 (r = 0.93, p < 0.01; Fig. 2c). Therefore, the HF treatment did not significantly change the original BC content.

Measurement for contents and carbon isotopes of TOC and BC. A total of 22 surface sediments (top 1–5 cm) and 2 sediment cores (29 samples) were analyzed. The contents and δ¹³C of TOC and BC were measured using a Vario Pyro Cube elemental analyzer and an Isoprime 100 continuous flow isotope ratio mass spectrometer, respectively. Acetanilide (IAEA) was used as an intra-lab reference standard for both carbon content (71.09%) and δ¹³C (–29.53‰). The TOC and BC contents were reported as weight percent of TOC (or BC) to dry weight sediment (wt.%), whereas δ¹³C was reported in per mil (‰) using δ notation relative to the Vienna Pee Dee Belemnite standard (VPDB). The average standard

deviation of each measurement, determined by replicate analyses, was $\pm 0.03\%$ for TOC or BC contents and $\pm 0.2\%$ for $\delta^{13}\text{C}$.

The $\Delta^{14}\text{C}$ of sedimentary TOC and BC was determined using AMS in the Center for Isotope Geochemistry and Geochronology (CIGC) at Qingdao National Laboratory for Marine Science and Technology, China (QNLM) and the Ocean University of China radioCarbon Accelerator Mass Spectrometer Center (OUC-CAMS). Part of samples containing $>50\ \mu\text{g C}$ were mixed with pre-combusted copper oxide (CuO) as an oxygen source and combusted into CO_2 at $900\ ^\circ\text{C}$ for 8 h using a vacuum line. The CO_2 was purified, quantified, graphitized using a zinc reduction method and then analyzed by AMS at the CIGC-QNLM. While for other samples containing carbon as low as $28\ \mu\text{g}$, they were combusted in an elemental analyzer (EA) and the product CO_2 was directly injected into the ion source of MICADAS through the Gas Interface System (GIS) at OUC-CAMS⁵⁹. All ^{14}C measurements were reported as fraction modern (Fm) and the conventional radiocarbon ages (year before present, BP) were calculated using the Libby half-life as previously described⁶⁰. Samples were normalized using oxalic acid II (NIST SRM4990C) and phthalic anhydride as a blank. The Fm precision of CO_2 gas measurements for the international standard oxalic acid II was better than $\pm 1\%$, whereas for the PhA, the Fm precision was $<10\%$ and Fm value was <0.005 ($\sim 42\ \text{ka B.P.}$). Radiocarbon values were corrected for procedural blanks with modern and dead standards known Fm values. Procedural blanks yield $1.50 \pm 0.38\ \mu\text{g C}$ with an Fm value of 0.47 ± 0.12 ($n = 8$).

Sedimentation rates in hadal trench regions. Because episodic mass wasting events can transport large quantities of sediments from the surrounding non-hadal area (e.g., trench slope) into the trench interior, steady-state accumulation in hadal trenches may have been interrupted by episodic events. Here, we used constant linear sedimentation rates previously reported^{16,21,37} that are based on excess ^{210}Pb activity ($^{210}\text{Pb}_{\text{ex}}$) in sediment cores by excluding mass wasting events (if any). The sedimentation rates vary from 0.08 to $0.16\ \text{cm yr}^{-1}$ in NBT, 0.13 to $0.20\ \text{cm yr}^{-1}$ in BT, 0.026 to $0.085\ \text{cm yr}^{-1}$ in AT, 0.030 to $0.042\ \text{cm yr}^{-1}$ in KT, and $0.038\ \text{cm yr}^{-1}$ in MT (Supplementary Table 5).

Estimating contributions of biomass (f_{biomass}) and fossil carbon (f_{fossil}). The BC in marine sediments can be derived from fossil fuel combustion, biomass burning and rock weathering^{10,42}. Since fossil fuel and rock weathering derived BC have overlapping $\delta^{13}\text{C}$ and $\Delta^{14}\text{C}$ signals⁴², we combined them as one endmember (fossil carbon) in the isotope mass-balance mixing model. The relative contribution to the BC from biomass burning (f_{biomass}) and fossil carbon (f_{fossil}) was calculated as following:

$$\Delta^{14}\text{C}_{\text{sed}} = \Delta^{14}\text{C}_{\text{biomass}} \times f_{\text{biomass}} + \Delta^{14}\text{C}_{\text{fossil}} \times f_{\text{fossil}} \quad (1)$$

$$1 = f_{\text{biomass}} + f_{\text{fossil}} \quad (2)$$

Here, $\Delta^{14}\text{C}_{\text{sediment}}$, $\Delta^{14}\text{C}_{\text{biomass}}$ and $\Delta^{14}\text{C}_{\text{fossil}}$ represent the radiocarbon activity of the BC in trench sediments, fresh biomass and fossil carbon, respectively. $\Delta^{14}\text{C}_{\text{biomass}}$ is similar to $\Delta^{14}\text{C}$ signal of modern atmospheric CO_2 that was assigned as $+50\%$, whereas $\Delta^{14}\text{C}_{\text{fossil}}$ was designated as -1000% since fossil carbon from the weathered rock and fossil fuel combustion is completely devoid of radiocarbon^{61,62}. Given high sedimentation rates in hadal trenches (0.026 – $0.20\ \text{cm yr}^{-1}$), the surface sediments (most top 5 cm) were deposited within the past <200 years that is much shorter than the half-life of ^{14}C age ($5730\ \text{yr}$). Thus, the ^{14}C ages were not corrected for the decay itself. Note that the pre-aged BC from soils and pre-deposited sediments characterized by intermediate ^{14}C ages between modern biomass and fossil carbon was not considered in our two-endmember mixing model due to the lack of endmember values, which may underestimate the contribution of biomass (f_{biomass}) to some extent.

Data availability

All methods and data supporting the findings of this study are available within the paper or its Supplementary Information Files (Supporting information.docx). Information is available in the Supplementary Data files, which are also deposited to the general data repository Figshare and can be accessed at <https://doi.org/10.6084/m9.figshare.16944808.v1>. The Supplementary Data 1–7 contain the source data for Figs. 1–7, respectively.

Received: 15 June 2021; Accepted: 20 January 2022;

Published online: 10 February 2022

References

- Schmidt, M. W. I. & Noack, A. G. Black carbon in soils and sediments: analysis, distribution, implications, and current challenges. *Global Biogeochem. Cycles* **14**, 777–793 (2000).
- Masiello, C. A. New directions in black carbon organic geochemistry. *Mar. Chem.* **92**, 201–213 (2004).
- Klimont, Z. et al. Global anthropogenic emissions of particulate matter including black carbon. *Atmos. Chem. Phys.* **17**, 8681–8723 (2017).
- Jones, M. W., Santín, C., van der Werf, G. R. & Doerr, S. H. Global fire emissions buffered by the production of pyrogenic carbon. *Nat. Geosci.* **12**, 742–747 (2019).
- Ogren, J. A. & Charlson, R. J. Elemental carbon in the atmosphere: cycle and lifetime. *Tellus B* **35B**, 241–254 (1983).
- Lohmann, R. et al. Fluxes of soot black carbon to South Atlantic sediments. *Global Biogeochem. Cycles* **23**, GB1015 (2009).
- Middelburg, J. J., Nieuwenhuize, J. & van Breugel, P. Black carbon in marine sediments. *Mar. Chem.* **65**, 245–252 (1999).
- Suman, D. O., Kuhlbusch, T. A. J., Lim, B. Marine Sediments: a reservoir for black carbon and their use as spatial and temporal records of combustion. In: *Sediment Records of Biomass Burning and Global Change* (eds Clark J. S., Cachier H., Goldammer J. G., Stocks B.). Springer Berlin Heidelberg (1997).
- Verardo, D. J. & Ruddiman, W. F. Late Pleistocene charcoal in tropical Atlantic deep-sea sediments: climatic and geochemical significance. *Geology* **24**, 855–857 (1996).
- Masiello, C. A. & Druffel, E. R. M. Black carbon in deep-sea sediments. *Science* **280**, 1911–1913 (1998).
- Ren, P. et al. Sources and sink of black carbon in Arctic Ocean sediments. *Sci. Total Environ.* **689**, 912–920 (2019).
- Wang, X. & Li, A. Preservation of black carbon in the shelf sediments of the East China Sea. *Chin. Sci. Bull.* **52**, 3155–3161 (2007).
- Qi, Y. et al. Dissolved black carbon is not likely a significant refractory organic carbon pool in rivers and oceans. *Nat. Commun.* **11**, 5051 (2020).
- Ziolkowski, L. A. & Druffel, E. R. M. Aged black carbon identified in marine dissolved organic carbon. *Geophys. Res. Lett.* **37**, L16601 (2010).
- Jamieson, A. *The hadal zone: life in the deepest oceans*. Cambridge University Press (2015).
- Sanei, H. et al. High mercury accumulation in deep-ocean hadal sediments. *Sci. Rep.* **11**, 10970 (2021).
- Itou, M., Matsumura, I. & Noriki, S. A large flux of particulate matter in the deep Japan Trench observed just after the 1994 Sanriku-Oki earthquake. *Deep Sea Res. I Oceanogr. Res. Pap.* **47**, 1987–1998 (2000).
- Oguri, K. et al. Hadal disturbance in the Japan Trench induced by the 2011 Tohoku-Oki Earthquake. *Sci. Rep.* **3**, 1915 (2013).
- Danovaro, R., Gambi, C. & Della Croce, N. Meiofauna hotspot in the Atacama Trench, eastern South Pacific Ocean. *Deep Sea Res. I Oceanogr. Res. Pap.* **49**, 843–857 (2002).
- Itoh, M. et al. Bathymetric patterns of meiofaunal abundance and biomass associated with the Kuril and Ryukyu trenches, western North Pacific Ocean. *Deep Sea Res. I Oceanogr. Res. Pap.* **58**, 86–97 (2011).
- Glud, R. N. et al. High rates of microbial carbon turnover in sediments in the deepest oceanic trench on Earth. *Nat. Geosci.* **6**, 284–288 (2013).
- Wenzhöfer, F. et al. Benthic carbon mineralization in hadal trenches: assessment by in situ O_2 microprofile measurements. *Deep Sea Res. I Oceanogr. Res. Pap.* **116**, 276–286 (2016).
- Glud, R. N. et al. Hadal trenches are dynamic hotspots for early diagenesis in the deep sea. *Commun. Earth Environ.* **2**, 21 (2021).
- Turnewitsch, R. et al. Recent sediment dynamics in hadal trenches: evidence for the influence of higher-frequency (tidal, near-inertial) fluid dynamics. *Deep Sea Res. I Oceanogr. Res. Pap.* **90**, 125–138 (2014).
- Ichino, M. C. et al. The distribution of benthic biomass in hadal trenches: a modelling approach to investigate the effect of vertical and lateral organic matter transport to the seafloor. *Deep Sea Res. I Oceanogr. Res. Pap.* **100**, 21–33 (2015).
- Kioka, A. et al. Event stratigraphy in a hadal oceanic trench: The Japan Trench as sedimentary archive recording recurrent giant subduction zone earthquakes and their role in organic carbon export to the Deep Sea. *Front. Earth Sci.* **7**, <https://doi.org/10.3389/feart.2019.00319> (2019).
- Meyers, P. A. Organic geochemical proxies of paleoceanographic, paleolimnologic, and paleoclimatic processes. *Org. Geochem.* **27**, 213–250 (1997).
- O’Leary, M. H. Carbon isotopes in photosynthesis: fractionation techniques may reveal new aspects of carbon dynamics in plants. *Bioscience* **38**, 328–336 (1988).
- Bird, M. I. & Ascough, P. L. Isotopes in pyrogenic carbon: a review. *Org. Geochem.* **42**, 1529–1539 (2012).
- Reddy, C. M. et al. Radiocarbon as a tool to apportion the sources of polycyclic aromatic hydrocarbons and black carbon in environmental samples. *Environ. Sci. Technol.* **36**, 1774–1782 (2002).
- Andersson, A. et al. Regionally-varying combustion sources of the January 2013 severe haze events over Eastern China. *Environ. Sci. Technol.* **49**, 2038–2043 (2015).

32. Behrenfeld, M. J. & Falkowski, P. G. Photosynthetic rates derived from satellite-based chlorophyll concentration. *Limnol. Oceanogr.* **42**, 1–20 (1997).
33. Giovanni, D. et al. Primary production and community respiration in the Humboldt Current System off Chile and associated oceanic areas. *Mar. Ecol. Prog. Ser.* **197**, 41–49 (2000).
34. Romero, H., Méndez, M. & Smith, P. Mining development and environmental injustice in the Atacama Desert of Northern Chile. *Environmen. Justice* **5**, 70–76 (2012).
35. Gallo, N. D. et al. Submersible- and lander-observed community patterns in the Mariana and New Britain trenches: influence of productivity and depth on epibenthic and scavenging communities. *Deep Sea Res. I Oceanogr. Res. Pap.* **99**, 119–133 (2015).
36. Li, D. et al. Comparison of sedimentary organic carbon loading in the Yap Trench and other marine environments. *J. Oceanol. Limnol.* **3**, <https://doi.org/10.1007/s00343-019-8365-9> (2019).
37. Luo, M. et al. Sources, degradation, and transfer of organic matter in the New Britain Shelf-Trench continuum, Papua New Guinea. *J. Geophys. Res. Biogeosci.* **124**, 1680–1695 (2019).
38. Xiao, W. et al. Efficient sequestration of terrigenous organic carbon in the New Britain Trench. *Chem. Geol.* **533**, 119446 (2020).
39. Xu, Y. et al. Glycerol dialkyl glycerol tetraethers in surface sediments from three Pacific trenches: Distribution, source and environmental implications. *Org. Geochem.* **147**, 104079 (2020).
40. Bao, R. et al. Tectonically-triggered sediment and carbon export to the Hadal zone. *Nat. Commun.* **9**, <https://doi.org/10.1038/s41467-017-02504-1> (2018).
41. Stewart, H. A. & Jamieson, A. J. Habitat heterogeneity of hadal trenches: considerations and implications for future studies. *Prog. Oceanogr.* **161**, 47–65 (2018).
42. Dickens, A. F., Gélinas, Y., Masiello, C. A., Wakeham, S. & Hedges, J. I. Reburial of fossil organic carbon in marine sediments. *Nature* **427**, 336–339 (2004).
43. Masiello, C. A. & Druffel, E. R. M. Organic and black carbon ¹³C and ¹⁴C through the Santa Monica Basin sediment oxic-anoxic transition. *Geophys. Res. Lett.* **30**, 1185 (2003).
44. Wagner, S. et al. Isotopic composition of oceanic dissolved black carbon reveals non-riverine source. *Nat. Commun.* **10**, 8 (2019).
45. Wagner, S. et al. Questions remain about the biolability of dissolved black carbon along the combustion continuum. *Nat. Commun.* **12**, 4281 (2021).
46. Blattmann, T. M., Liu, Z., Zhang, Y., Zhao, Y. & Eglinton, T. I. Mineralogical control on the fate of continentally derived organic matter in the ocean. *Science* **366**, 742–745 (2019).
47. Schmidt, M. W. I. et al. Persistence of soil organic matter as an ecosystem property. *Nature* **478**, 49–56 (2011).
48. Salvadó, J. A., Bröder, L., Andersson, A., Semiletov, I. P. & Gustafsson, Ö. Release of black carbon from thawing permafrost estimated by sequestration fluxes in the East Siberian Arctic shelf recipient. *Global Biogeochem. Cycles* **31**, 1501–1515 (2017).
49. Qi, L. & Wang, S. Fossil fuel combustion and biomass burning sources of global black carbon from GEOS-Chem simulation and carbon isotope measurements. *Atmos. Chem. Phys.* **19**, 11545–11557 (2019).
50. Völker, D. et al. Latitudinal variation in sedimentary processes in the Peru-Chile Trench off Central Chile. In: *The Andes: Active Subduction Orogeny* (eds Oncken O. et al.). Springer Berlin Heidelberg (2006).
51. Fang, Y. et al. Large-river dominated black carbon flux and budget: a case study of the estuarine-inner shelf of East China Sea, China. *Sci. Total Environ.* **651**, 2489–2496 (2019).
52. Fang, Y. et al. Flux and budget of BC in the continental shelf seas adjacent to Chinese high BC emission source regions. *Global Biogeochem. Cycles* **29**, 957–972 (2015).
53. Smith, D. M., Griffin, J. J. & Goldberg, E. D. Elemental carbon in marine sediments: a baseline for burning. *Nature* **241**, 268–270 (1973).
54. Jamieson, A. J., Malkocs, T., Piertney, S. B., Fujii, T. & Zhang, Z. Bioaccumulation of persistent organic pollutants in the deepest ocean fauna. *Nature Ecol. Evol.* **1**, 51 (2017).
55. Kioka, A. et al. Megathrust earthquake drives drastic organic carbon supply to the hadal trench. *Sci. Rep.* **9**, 1553 (2019).
56. Clift, P. D. A revised budget for Cenozoic sedimentary carbon subduction. *Rev. Geophys.* **55**, 97–125 (2017).
57. Gustafsson, Ö., Haghseta, F., Chan, C., MacFarlane, J. & Gschwend, P. M. Quantification of the dilute sedimentary soot phase: implications for PAH speciation and bioavailability. *Environ. Sci. Technol.* **31**, 203–209 (1997).
58. Gélinas, Y., Prentice, K. M., Baldock, J. A. & Hedges, J. I. An improved thermal oxidation method for the quantification of soot/graphitic black carbon in sediments and soils. *Environ. Sci. Technol.* **35**, 3519–3525 (2001).
59. McIntyre, C. P. et al. Online ¹³C and ¹⁴C gas measurements by EA-IRMS-AMS at ETH Zürich. *Radiocarbon* **59**, 893–903 (2017).
60. Stuiver, M. & Polach, H. A. Discussion: reporting of ¹⁴C data. *Radiocarbon* **19**, 355–363 (1977).
61. Turnbull, J. C. et al. Sixty years of radiocarbon dioxide measurements at Wellington, New Zealand: 1954–2014. *Atmos. Chem. Phys.* **17**, 14771–14784 (2017).
62. Dasari, S. et al. Source quantification of south Asian black carbon aerosols with isotopes and modeling. *Environ. Sci. Technol.* **54**, 11771–11779 (2020).
63. Schlitzer, R. Ocean Data View. <https://odv.awi.de> (2021).
64. Smith, R. W., Bianchi, T. S., Allison, M., Savage, C. & Galy, V. High rates of organic carbon burial in fjord sediments globally. *Nat. Geosci.* **8**, 450–453 (2015).

Acknowledgements

This work is financially supported from the National Natural Science Foundation of China (41976030, 42076029, 91951210), the Open Research Fund of State Key Laboratory of Estuarine and Coastal Research (#SKLEC-KF202108), the China Postdoctoral Science Foundation (2020M682768), and the Danish National Research Foundation grant DNR145 via the Danish Center for Hadal Research. Wenjie Xiao thanks the support of SUSTech Presidential Postdoctoral Fellowship and Shanghai Sheshan National Geophysical Observatory (Grant 2020Z01). Samples were obtained during cruises by the RV SONNE, cruise SO261, RV Tangaroa, cruise TAN1711, and RV Zhangjian, cruise 11,000 m sea trial. The voyages were made by the HADES-ERC Advanced grant (669947), the Coasts & Oceans Center of New Zealand's National Institute of Water & Atmospheric Research (TAN1711), and the Shanghai Engineering Research Center of Hadal Science and Technology (15DZ1207000). We thank captain(s), crew(s), and scientific personnel for their excellent support to obtain these samples. Anni Glud, Mathias Zabel, Binbin Pan and Weicheng Cui are thanked for onboard assistance, cruise preparation and organization. This is OUC-CAMS contribution #4.

Author contributions

Y.X. conceived the original concept and coordinated the research, F.W., A.R., R.N.G., and Y.X. organized the cruises and collected samples. X.Z., W.X., X.L., M.L., K.O., M.Z., Z.W., X.W., L.X., Y.F. and Y.W. conducted the laboratory analyses. Y.X., W.X., R.N.G., F.W., A.R., S.M., J.F. and Y.F. discussed the data and wrote the manuscript. All authors read, edited, and approved the final version of the manuscript.

Competing interests

The authors declare no competing interests.

Additional information

Supplementary information The online version contains supplementary material available at <https://doi.org/10.1038/s43247-022-00351-7>.

Correspondence and requests for materials should be addressed to Yunping Xu or Wenjie Xiao.

Peer review information *Communications Earth & Environment* thanks Rainer Lohmann and the other, anonymous, reviewer(s) for their contribution to the peer review of this work. Primary Handling Editors: Mojtaba Fakhraee and Clare Davis. Peer reviewer reports are available.

Reprints and permission information is available at <http://www.nature.com/reprints>

Publisher's note Springer Nature remains neutral with regard to jurisdictional claims in published maps and institutional affiliations.



Open Access This article is licensed under a Creative Commons Attribution 4.0 International License, which permits use, sharing, adaptation, distribution and reproduction in any medium or format, as long as you give appropriate credit to the original author(s) and the source, provide a link to the Creative Commons license, and indicate if changes were made. The images or other third party material in this article are included in the article's Creative Commons license, unless indicated otherwise in a credit line to the material. If material is not included in the article's Creative Commons license and your intended use is not permitted by statutory regulation or exceeds the permitted use, you will need to obtain permission directly from the copyright holder. To view a copy of this license, visit <http://creativecommons.org/licenses/by/4.0/>.

© The Author(s) 2022